



ARTICLE

The Effect of Basalt Fiber on Concrete Performance under a Sulfate Attack Environment

Qiang Su and Jinming Xu*

Department of Civil Engineering, Shanghai University, Shanghai, 200444, China

*Corresponding Author: Jinming Xu. Email: xjming211@163.com

Received: 01 December 2021 Accepted: 12 January 2022

ABSTRACT

To enhance the sulfate attack resistance performance of concrete, Sulfate erosion test was carried out on basalt fiber concrete with different contents, selecting a concentration of 5% sulfate solution and using a dry-wet cycle mechanism attack of basalt fiber-reinforced concrete (BFRC). Every 15 dry-wet cycles, the mass, compressive strength, splitting tensile strength, and relative dynamic elastic modulus of BFRC were tested, and the SO_4^{2-} concentration was measured. This work demonstrates that the mass, relative dynamic elastic modulus, compressive and splitting tensile strength of BFRC reveal a trend of climb up and then decline with the process of the dry-wet cycle. Basalt fiber can enhance the sulfate corrosion resistance of concrete by delaying the erosion of concrete induced by SO_4^{2-} and increasing the bearing and anti-deformation capacities of concrete by improving its internal structure. Additionally, when mixing 0.2% basalt fiber into concrete, the strength deterioration rate will be reduced when the peak values of splitting tensile and compressive strength appear at 60 and 75 times the alternating dry-wet cycles, respectively. Adverse effects will occur when the fiber volume fraction exceeds 0.2%. The research in this paper can provide a foundation for the engineering applications of basalt fiber concrete.

KEYWORDS

Concrete; basalt fiber; dry-wet cycle; compressive strength; splitting tensile strength

1 Introduction

Concrete is the most widely used, basic building material in the world. It is increasingly used in civil engineering, transportation, water conservancy, and hydropower. At present, the durability of concrete structures corroded by sulfate has been widely studied. The essence of the mechanism of sulfate attack concrete is SO_4^{2-} in the external erosion medium through microcracks in the concrete's surface to the interior of concrete pores under natural conditions. A chemical reaction with the components in cement stone leads to the expansion of concrete's volume. When the expansion's internal stress exceeds the tensile strength of the concrete, the concrete cracks further, causing more SO_4^{2-} to enter concrete, aggravating the expansion of the volume, making the concrete crack increasingly serious, and leading to the destruction of concrete structures [1,2]. Gao et al. [3] conducted a durability test of concrete under the action of sulfate. The corrosion mechanism and influence law on concrete strength were analyzed. Gao et al. [4] studied the attack process of sulfate on concrete under bending load and dry-wet cycles. The results demonstrated that, compared with the single failure process of sulfate attack, both bending load



and dry–wet cycles could accelerate the failure process of concrete attacked by sulfate. Compared with sulfate attack and dry–wet cycles, the effect of bending load on concrete deterioration depends on the stress level. Bassuoni et al. [5] researched the sulfate attack resistance of concrete under the action of dry–wet cycles and bending loads. They found that, under this combined action, the mechanism of action was quite different between the concrete's corrosion and the single failure mechanism (sulfate attack) of concrete. Through the shear test and microscopic scanning of concrete specimens subjected to sulfate attack in various periods, Zhang et al. [6] analyzed the influence mechanism of sulfate attack on the shear strength and failure mode of concrete with semi-immersion. The sulfate attack led to the degradation of concrete's shear strength. With the increased exposure time, the representation of cohesion and the shear expansion rate of the concrete's shear strength revealed a trend of gradual decrease. Jiang et al. [7] studied the thickness change rule and microscopic analysis of concrete's damage layer under the action of sulfate attack. They illustrated that, as the water–binder ratio increased, the ettringite and gypsum in concrete continuously increased and the calcium hydroxide content slowly decreased. The macroscopic performance depicts that the ultrasonic velocity in the concrete damage layer gradually decreases and the thickness of the damage layer increases.

Basalt fiber is a natural, inorganic, non-metallic material. Mixing basalt fiber into concrete can form a certain tension inside the concrete, make it more compact, and augment its mechanical properties, chemical stability, and corrosion resistance [8]. In recent years, basalt fiber-reinforced concrete (BFRC), a new type of cement-based composite material, has been widely used in marine construction, expressways, and projects in harsh environments due to its better comprehensive performance. To provide relevant theoretical references for diverse engineering needs, scholars have carried out in-depth research on the mechanical properties and durability of BFRC. A research on the recycled BFRC strengths was done by Huang et al. [9]. After adding basalt fiber, they demonstrated that the splitting tensile and flexural strength of recycled concrete significantly ameliorated, while the compressive strength climb up and then decline. Wang et al. [10] showed that the prophase of shrinkage cracks decreased with the increased basalt fiber content, and no cracks were observed when the basalt fiber content was 0.20%. Li et al. [11] analyzed the influence of disparate kinds of fibers on the impact performance of concrete and discovered that the influence of basalt fiber is generally better than that of carbon fiber, which can improve the impact strength and toughness of concrete. Yang et al. [12] investigated the influence of basalt fiber volume fraction on the strength and damage of concrete. The results depicted that mixing basalt fiber can slow down the prophase of cracking and weaken the transverse strain of concrete. With the heightened basalt fiber volume fraction, the macro cracks on the surface of concrete gradually transformed into a large number of micro ones. Chen et al. [13] examined the influences of fiber content, fiber length, and fiber diameter on the splitting tensile and compressive strength of basalt fiber concrete using orthogonal testing. Their results proved that the changed content of basalt fiber was significantly influential in the mechanical properties of concrete, and the optimal fiber content and fiber size were determined through their test. Branston et al. [14] did a research on the early performance of basalt fiber concrete, revealing that an appropriate amount of basalt fiber can effectively prevent segregation, enhance the water retentivity and cohesion of concrete, and reduce early shrinkage, which has a significant influence on inhibiting the early cracking of concrete. Jung et al. [15] conducted an experimental analysis on the chemical composition and stability of basalt fiber in alkaline solution. They found that basalt fiber has good resistance to weak alkali attacks and stable chemical composition. Jalsutram et al. [16] experimented on the strength and deformation of basalt fiber concrete. They found that an proper quantity of basalt fiber can play a positive role in the deformation capacity of concrete.

In summary, the current research on the durability and corrosion mechanism of ordinary concrete is relatively mature. There are some research results on the mechanical behavior of basalt fiber concrete, but the experimental research on the durability of basalt fiber concrete, especially in sulfate attack

environments, is relatively limited. Mixing a certain amount of basalt fiber into concrete can enhance its corrosion resistance, but its mechanical properties will still degrade to a certain degree. There are relatively few studies on the degree of degradation and the law of corrosion. Sulfate is widespread in nature, so sulfate corrosion is a challenge that many structural engineers must face. With the infiltration of SO_4^{2-} , it will have a significant effect on internal materials. Through the corrosion test of a 5% sodium sulfate solution, this paper studies the mass, compressive strength, splitting tensile strength, relative dynamic elastic modulus, and SO_4^{2-} distribution of BFRC under sulfate attack. With SEM microscopic tests, the law of strength degradation during and after the corrosion of concrete is revealed. Subsequently, a strength degradation model is proposed to provide technical support for the application of basalt fiber concrete in a sulfate environment.

2 Materials and Methods

2.1 Raw Materials

The binder used in the test was Chinese standard Portland cement. The 28-d compressive strength was 42.5 MPa. The fine aggregate was natural river sand, which belongs to medium sand with a fineness modulus of 2.8. The coarse aggregate was a continuous graded crushed stone with a particle size of 5–20 mm. Chopped basalt fiber was selected as the fiber, and the physical and mechanical performance parameters are illustrated in [Table 1](#). The sulfate was an analytical reagent sodium sulfate anhydrous. The water-reducing agent was high-performance HPWR liquid-type water-reducing agent, with a water-reduction rate of 37%. Ordinary tap water was used.

Table 1: Physical and mechanical performance parameters of chopped basalt fiber

Diameter (μm)	Length (mm)	Tensile strength (MPa)	Density (kg/m^3)	Ultimate elongation (%)	Elastic modulus (GPa)
12	18	4600	2650	2.8	84.6

2.2 Mix Proportion Design

To study the performance of BFRC in a sulfate attack environment, seven groups of concrete with different volume contents of basalt fiber were designed. The content of basalt fiber was 0%, 0.05%, 0.1%, 0.15%, 0.2%, 0.25%, and 0.3%, respectively. The mixing amount of the water-reducing agent was determined according to the workability. The specific mix proportion of BFRC is depicted in [Table 2](#).

Table 2: Mix proportion of BFRC

Cement	Coarse aggregate	Fine aggregate	Water	Water-reducing agent
430	1185	650	195	5.25

2.3 Specimen Preparation

A forced mixer was used to make the specimens. First, the weighed stones and sand were mixed and dry-mixed for 90 s. Subsequently, the basalt fiber was added to continue dry mixing for 90 s. Cement was added to continue dry mixing for 120 s, and finally, water and water-reducing agents were added and mixed for 120 s to complete the production of BFRC. The cube specimens with a size of 100 mm \times 100 mm \times 100 mm were placed into a non-flowing saturated calcium hydroxide solution at a room temperature of $20 \pm 2^\circ\text{C}$ for curing for 28 d.

2.4 Methods

The concentration of sulfate solution in this test was 5%, and the specimen was put into sulfate solution for a dry–wet cycle after curing. To fully erode the specimen and to avoid physical damage to the concrete and changes in the erosion mechanism during drying, the cycle scheme adopted was soaking for 54 h, taking out and drying the surface moisture, drying for 18 h, and setting the drying temperature to 85°C, which is regarded as a cycle. The test pieces were taken out after zero, 15, 30, 45, 60, 75, 90, 105, and 120 cycles. The researchers tested the mass, compressive strength, splitting tensile strength, and relative dynamic elastic modulus.

The instrument used for the compressive strength and splitting tensile strength test was the WAW-2000D electro-hydraulic servo universal testing machine. The loading rate was 0.5 MPa/s and 0.05 MP/s, respectively, and the failure conditions were unified when the bearing capacity decreased by 85% and the loading was stopped.

The corrosion resistance coefficients of compressive strength and splitting tensile strength are important indexes for evaluating the sulfate resistance performance of concrete. The design formula is provided in Eq. (1):

$$K = \frac{f_n}{f_0} \quad (1)$$

where K represents the corrosion resistance coefficient of compressive strength or splitting tensile strength, f_n represents the compressive strength or splitting tensile strength of the specimen after n times of the dry–wet cycle (MPa), and f_0 represents the compressive strength or splitting tensile strength of the specimen without a dry–wet cycle (MPa).

The SO_4^{2-} concentration of the concrete selection water-soluble extraction method [17–19]. The eroded specimens were sliced (each piece of concrete thickness was 12 mm). In addition, the concrete specimens sliced by the HDM-1A concrete grinder were used for stratified sampling; that is, the slice depth of the specimen was 0~12 mm, 12~24 mm, 24~36 mm, and 36~48 mm, respectively. The sliced specimens of different depths were ground into powder, passed through a 0.16 mm square-hole sieve, and then collected and dissolved in water. The concentration of SO_4^{2-} was determined by an SY-3 sulfate rapid tester.

The dynamic elastic modulus of concrete was assessed with the DT-W18 dynamic elastic modulus tester. First, the size and mass of the concrete were measured. Next, the tester was adjusted to achieve the resonance state. At this time, the resonance frequency displayed by the tester was the initial vibration frequency of the test piece. The dynamic elastic modulus design formula is illustrated in Eq. (2).

$$E_d = 13.244 \times 10^{-4} \times \frac{WL^3f^2}{a^4} \quad (2)$$

where E_d represents the dynamic elastic modulus of the test piece (MPa); a represents the side length of the section of the test piece (mm); L represents the length of the test piece (mm); W represents the mass of the test piece, accurate to 0.01 kg (kg); and f represents the fundamental vibration frequency of the test piece (Hz).

The relative dynamic elastic modulus design formula is given in Eq. (3).

$$E = \frac{E_{di}}{E_{0i}} \quad (3)$$

where E represents the relative dynamic elastic modulus of the test piece, E_{di} represents the dynamic elastic modulus of the i -th concrete test piece after the dry–wet cycles (MPa), and E_{0i} represents the dynamic elastic modulus of the i -th concrete test piece before the dry–wet cycles (MPa).

3 Results and Discussion

3.1 Compressive Strength and Splitting Tensile Strength

The compressive strength values and the splitting tensile strength values of BFRC under various cycle times of the dry–wet cycle in a sulfate attack environment are shown in Figs. 1a and 1b.

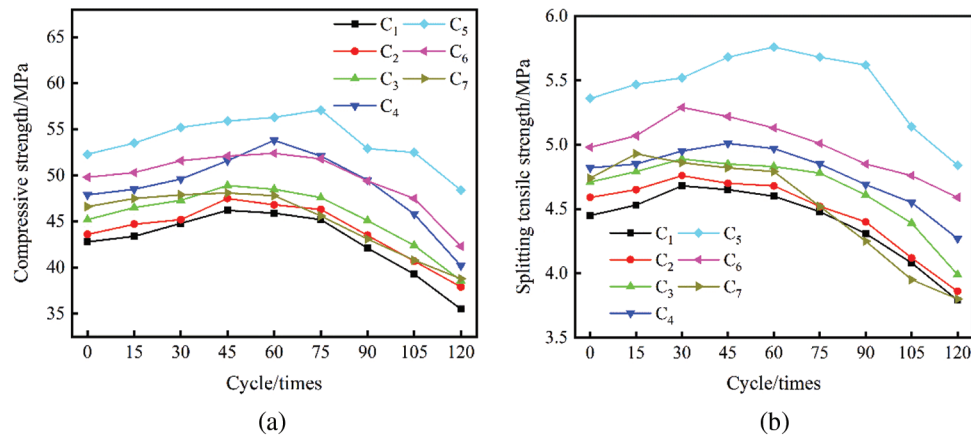


Figure 1: Variation law of BFRC strength with the number of dry–wet cycles

As can be seen from Fig. 1a, the compressive strength of the specimens in groups C₁, C₂, C₃, and C₇ reached their peak values at 45 dry–wet cycles. Compared with the specimens without the dry–wet cycle, the compressive strength of each group increased by 7.94%, 8.94%, 8.19%, and 3.22%, respectively. The compressive strength of the specimens in groups C₄ and C₆ reached their peak value at 60 dry–wet cycles. Compared with the specimens without the dry–wet cycle, the compressive strength raised by 12.32% and 5.22%, respectively. The peak value of compressive strength of the specimens in group C₅ appeared at the latest, at 75 dry–wet cycles, which was 9.18% more than that of specimens without dry–wet cycles. After the compressive strength of the above groups of specimens reached their peak value, the compressive strength gradually decreased as dry–wet cycles continued. With 120 dry–wet cycles, compared with those without dry–wet cycles, the compressive strength of specimens in groups C₁ to C₇ decreased by 17.06%, 13.07%, 14.6%, 16.08%, 7.46%, 15.06%, and 20.1%, respectively.

As seen in Fig. 1b, the splitting tensile strength of specimens in groups C₁, C₂, C₃, and C₆ reached their peak value at 30 dry–wet cycles. Compared with the specimens without the dry–wet cycle, the splitting tensile strength of each group increased by 5.17%, 3.7%, 3.82%, and 6.22%, respectively. The splitting tensile strength of the specimens in group C₄ reached their peak value at 45 dry–wet cycles, an increase of 3.94% compared with the specimens without dry–wet cycles. The peak value of the splitting tensile strength of the specimens in group C₅ appeared the latest, at 60 dry–wet cycles, an increase of 7.46% compared to the specimens without dry–wet cycles. The splitting tensile strength of group C₇ specimens reached their peak value at 15 dry–wet cycles, increasing by 4.01%. After the splitting tensile strength of the above groups of specimens attained their peak value, the splitting tensile strength gradually decreased as dry–wet cycles continued. With 120 dry–wet cycles, compared with those without dry–wet cycles, the splitting tensile strength of the specimens decreased by 14.83%, 15.9%, 15.29%, 11.41%, 7.83%, 9.7%, and 19.83%, respectively.

In summary, it can be seen that (1) for the specimens without a dry–wet cycle, mixing basalt fiber into concrete can improve the compressive strength and splitting tensile strength of concrete to a certain extent. The strength performance was the best when the volume ratio of basalt fiber was 0.2%. Compared with

concrete without basalt fiber, the compressive strength and splitting tensile strength improved by 22.2% and 20.45%, respectively. (2) Basalt fiber can improve the sulfate attack resistance of concrete and delay the damage of SO_4^{2-} ions to the interior of concrete to a certain extent. This is because basalt fiber has a good crack resistance effect in concrete. It can effectively delay the attack of SO_4^{2-} and help inhibit the cracking of concrete [19–21]. (3) The specimens in group C_5 displayed the best performance under different dry–wet cycles in a sulfate attack environment.

Through the performance of BFRC's strength under assorted dry–wet cycles in the sulfate attack environment, the sulfate attack of BFRC was roughly divided into two stages. In the first stage, the generated ettringite, gypsum, and precipitated salt filled the internal pores of BFRC, which produced a certain expanded internal stress but not enough to produce expansion cracks. Conversely, to a certain extent, crystals, such as ettringite, filled the internal pores of BFRC and became one of the framework materials that constitute BFRC, bettering BFRC's compactness and strength. In the second stage, there were no more pores inside the BFRC to contain these products. The continuously generated ettringite and gypsum formed greater internal stress inside the BFRC, accelerating the formation and expansion of BFRC cracks. Simultaneously, due to the action of dry–wet cycles, when the mass fraction of sodium sulfate in the pores exceeded its solubility, white $\text{Na}_2\text{SO}_4 \cdot 10\text{H}_2\text{O}$ crystals precipitated and formed great crystallization pressure inside the BFRC. The cross-action of these internal stresses caused the BFRC to expand and crack, making it easier for the external SO_4^{2-} to penetrate the inside of the BFRC. Such processes were conducted alternately and promoted each other, forming a vicious circle that gradually reduced BFRC's strength.

3.2 Corrosion Resistant Coefficient for Compressive and Splitting Tensile Strength

Fig. 2 shows the calculation results of the corrosion resistant coefficient for BFRC strength. Fig. 2a demonstrates that the corrosion resistant coefficient for compressive strength climb up and then decline with dry–wet cycles, explained that the specimens had a certain resistance to sulfate attack in the early stage of the dry–wet cycles. When the dry–wet cycles reached 90 iterations, the corrosion resistant coefficient for compressive strength of the specimens of groups C_1 , C_2 , C_3 , and C_6 were lower than one, indicating that the degree of internal deterioration above the four groups of specimens was more serious and the sulfate attack resistance was low. The corrosion resistant coefficient for compressive strength of the specimens of groups C_7 was lower than one when the dry–wet cycles were repeated 75 times. The corrosion resistant coefficient for compressive strength of the specimens of groups C_4 was less than one when the dry–wet cycles occurred 105 times. The corrosion resistant coefficient for compressive strength of the specimens of groups C_5 was lower than one with 120 dry–wet cycles. The corrosion resistant coefficient for compressive strength of the specimens of groups C_1 to C_7 were 0.8294, 0.8693, 0.854, 0.8392, 0.9254, 0.8494, and 0.8326, respectively. Fig. 2b shows that the corrosion resistant coefficient for splitting tensile strength of the specimens of each group was generally consistent with the performance of the corrosion resistant coefficient for compressive strength as the dry–wet cycles proceeded, and not repeated here. The distinction is that the corrosion resistant coefficient for the splitting tensile strength of each specimen group decreased faster than the corrosion resistant coefficient for compressive strength, revealing that the enhancement influence of basalt fiber on the compressive strength of specimens under dry–wet cycle role in a sulfate attack environment was greater than that of splitting tensile strength.

In summary, an appropriate amount of basalt fiber mixed into concrete is beneficial for improving its sulfate resistance and delaying the corrosion damage of SO_4^{2-} to concrete to a certain extent. When excessive basalt fiber is mixed in, the effect is poor.

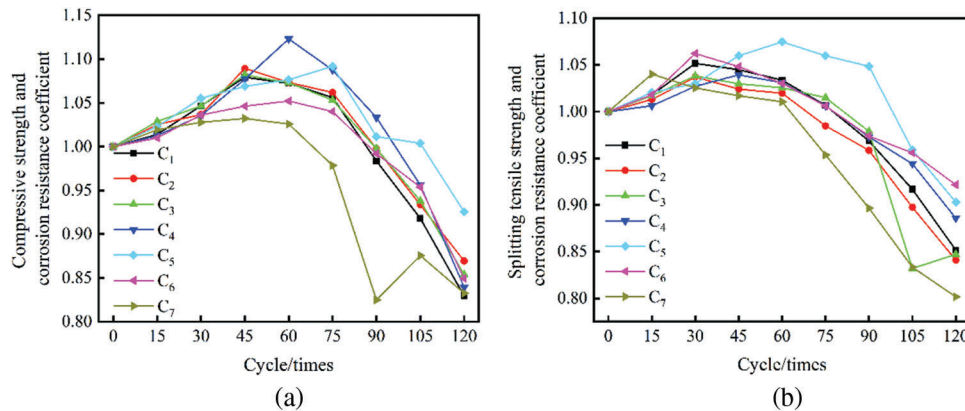


Figure 2: Variation in the corrosion resistance coefficient of compressive strength and splitting tensile strength of BFRC with the number of dry–wet cycles

3.3 Mass

The mass of the BFRC varied with the number of dry–wet cycles, as illustrated in Fig. 3. Fig. 3 reveals that the mass of BFRC changes with the number of dry–wet cycles, mainly divided into two stages. That is, it rapidly increases first and then rapidly or oscillatorily declines. The mass of specimens of groups C₁, C₂, and C₃ all increased rapidly before 45 dry–wet cycles, the mass of specimens of groups C₄, C₆, and C₇ increased rapidly before 60 dry–wet cycles, and the mass of specimens of group C₅ all increased before 75 dry–wet cycles. This was due to the chemical reaction between sulfate ions and cement hydration in the early stage of corrosive to produce swelling corrosive substances, which filled the internal pores of the specimens. The largest increases in the mass of specimens in groups C₁ and C₅ were 8.92% and 9.83%, respectively. After that, the mass of specimens in each group decreased rapidly or was oscillated. This is due to the large-area sanding and local spalling under the corrosive effect, causing internal damage to the specimens and mass decline. Among them, the mass of specimens in groups C₁ and C₅ decreased by 8.65% and 3.34%, respectively, compared with that without sulfate attack after 120 dry–wet cycles.

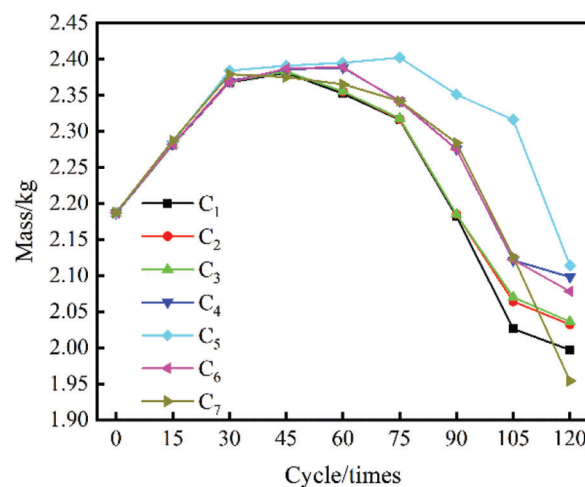


Figure 3: The mass of BFRC varies with the number of dry–wet cycles

3.4 Relative Dynamic Modulus of Elasticity

The change rule of the relative dynamic elastic modulus of each group of specimens under the action of dry–wet cycles in a sulfate attack environment is shown in Fig. 4. The relative dynamic elastic modulus of each group of specimens showed a trend of increases first and then decreases. After 120 dry–wet cycles, the relative dynamic elastic modulus of specimens in groups C₁ to C₇ decreased by 30.2%, 27.4%, 24.4%, 13.6%, 10.6%, 26.6%, and 31.6%, respectively. Under the dry–wet cycles. In a sulfate attack environment, the degree of deterioration damage of specimens in group C₅ was the smallest, and the relative dynamic elastic modulus of group C₇ was closer to that of group C₁, but slightly less than that of ordinary concrete, indicating that the degree of deterioration damage was more serious than that of ordinary concrete.

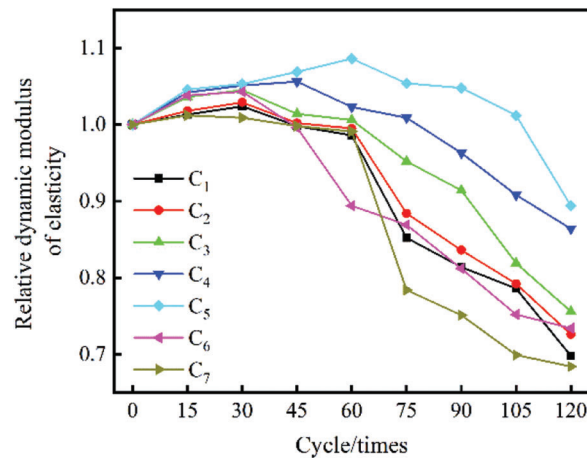


Figure 4: The relative dynamic elastic modulus of BFRC varies with the number of dry–wet cycles

3.5 SO_4^{2-} Concentration Distribution

Fig. 5 shows the change rule of BFRC's SO_4^{2-} content when dry–wet cycles were repeated 60 times. The concentration of SO_4^{2-} in each group shows a downward trend. The decline rate gets increasingly faster with depth, and the content of SO_4^{2-} gradually decreases with greater penetration depth. Because the surface of BFRC inhales a large amount of solution within the range of the influence depth, the concentration of SO_4^{2-} on the surface of BFRC was relatively high. As the depth increased, the migration rate of SO_4^{2-} decreased, and the concentration decreased accordingly.

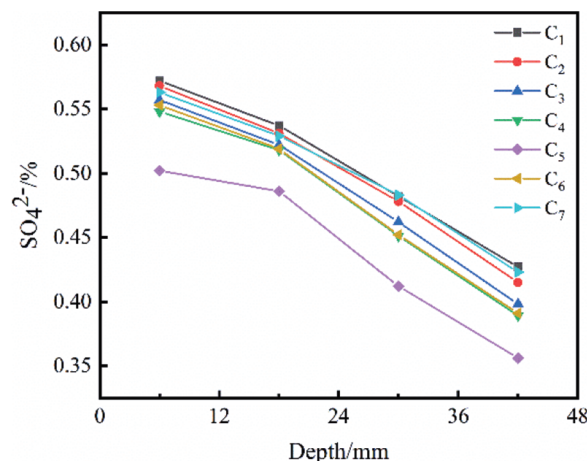


Figure 5: The change rule of the SO_4^{2-} content of BFRC at 60 dry–wet cycles

Fig. 6 reveals the change rule of the SO_4^{2-} content of BFRC with 120 dry–wet cycles. The SO_4^{2-} concentration of each group of specimens still showed a downward trend, with decreases slow in the early stage and the latter decreasing rapidly. After 120 dry–wet cycles, the SO_4^{2-} concentration of each group of specimens was higher than that of 60 dry–wet cycles. The mass fraction of SO_4^{2-} from the outer layer to the inner layer also gradually decreased.

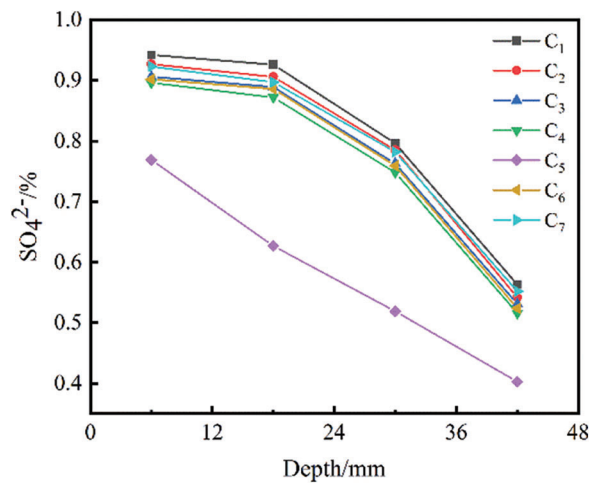


Figure 6: The change rule of the SO_4^{2-} content of BFRC at 120 dry–wet cycles

Based on Figs. 5 and 6, mixing basalt fiber into concrete significantly reduces the SO_4^{2-} concentration at different depths inside the concrete. The SO_4^{2-} corrosion resistance of concrete is in the order of group $C_5 > \text{group } C_4 > \text{group } C_6 > \text{group } C_3 > \text{group } C_7 > \text{group } C_2 > \text{group } C_1$, which indicates that mixing the appropriate amount of basalt fiber into the concrete can improve the SO_4^{2-} corrosion resistance of concrete and reduce the intrusion of SO_4^{2-} . Excessive basalt fiber mixed into concrete has a poor effect. If only from the perspective of reducing the SO_4^{2-} concentration at different depths inside the BFRC, it is recommended that the basalt fiber content be 0.2%.

4 Microstructure and Damage Deterioration Mechanism of BFRC

To deeply study the corrosion mechanism of BFRC under the action of dry–wet cycles in the sulfate attack environment, the core parts of specimens of groups C_1 and C_5 were selected for SEM scanning at zero and 120 dry–wet cycles, as shown in Figs. 7 and 8.

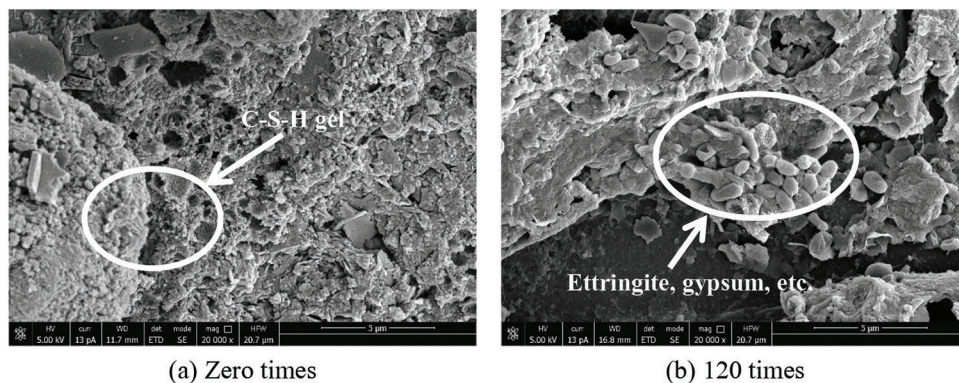


Figure 7: Microstructure of group C_1 specimens under different iterations of dry–wet cycles

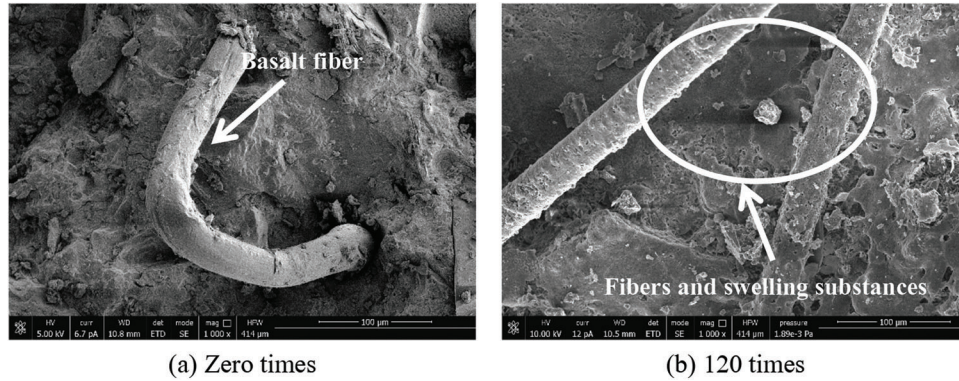


Figure 8: Microstructure of the specimens of group C_5 under diverse repetitions of dry–wet cycles

Figs. 7 and 8 demonstrate the surface of specimens without dry–wet cycles was covered with spherical or dense spinous substances, mainly cement hydrating substrates (C-S-H gel). When the specimen was subjected to external load, it could form a certain mechanical bite force with the cement matrix and that the single fiber is dispersed in the sample and acts as a reinforcing bar, playing the role of secondary micro-reinforcement. Simultaneously, the three-dimensional network structure formed by the fiber interaction and the bridging influence of fiber strengthened the bonding between the matrix and the fiber, can improving the mechanical properties of the specimen. However, once you have an excess of fiber will lead to fiber agglomeration, reducing the compactness of concrete, affecting the full bonding between the fibers and the matrix, increasing the internal defects of specimens, and ultimately leading to decreased strength in specimens. During the dry–wet cycles, the sulfate ion in the corrosion medium penetrated the specimen through the internal pores and reacted with the cement hydration products to produce expansive substances such as gypsum and ettringite. The content increased. Meanwhile, salt crystals precipitated in the corrosion process also kept increasing. In the initial stage of corrosion, these products can work together with the concrete matrix and, to some extent, become part of the concrete skeleton to improve the mechanical properties of specimens. However, the inside of the specimen slowly does not have sufficient pores to accommodate these continuously generated expansive substances and salts due to continuous sulfate corrosion, leading to large stress inside the specimen, causing cracks inside the concrete, and accelerating its expansion over time. Therefore, as the dry–wet cycles progressed, the deterioration degree of the specimens became increasingly serious, and the sulfate attack resistance was reduced.

5 Strength Deterioration Model of BFRC

To establish the strength deterioration model under the influence parameters of dry–wet cycle times and basalt fiber content, according to the test data of the compressive strength and split tensile strength of BFRC, the least squares method [22,23] was used to conduct regression analysis on the BFRC strength test within 120 dry–wet cycles. The compressive strength deterioration model of BFRC was obtained as shown in Eq. (4), and the splitting tensile strength deterioration model is depicted in Eq. (5).

$$f_{cc} = 42.65 - 47.79x + 0.1197y + 965.2x^2 + 0.1247xy - 0.0005795y^2 - 2568x^3 - 1.074x^2y + 0.001436xy^2 \quad (4)$$

$$f_{ts} = 4.545 - 7.209x + 0.009096y + 105.4x^2 + 0.03789xy - 0.0001255y^2 - 265.7x^3 - 0.1468x^2y \quad (5)$$

where f_{cc} is the compressive strength of BFRC (MPa), f_{ts} is the splitting tensile strength of BFRC (MPa), x is the fiber content (%), and y is the number of dry–wet cycles (times).

6 Conclusion

- (1) The mass, compressive strength, splitting tensile strength, and relative dynamic elastic modulus of BFRC increased first and then decreased with the number of dry–wet cycles in a sulfate attack environment.
- (2) The addition of basalt fiber to concrete can effectively improve the sulfate attack resistance of concrete, delay the corrosion of sulfate ions on specimens, and significantly improve the internal pores and crack expansion of concrete. An appropriate amount of basalt fiber can reduce the internal pores of concrete, but the excessive addition of basalt fiber makes no obvious improvement on the magnesium sulfate attack resistance of concrete. Indeed, it even decreases. When the content of basalt fiber is 0.2%, the sulfate resistance of concrete is most obviously improved.
- (3) When the content of basalt fiber is 0.2%, with the sulfate attack processes, the compressive strength and mass will both reach their peak value at 75 dry–wet cycles. The splitting tensile strength will reach its peak value at 60 iterations. After 120 dry–wet cycles, the decrease in the relative dynamic elastic modulus reached its lowest, at 10.6%.
- (4) Mixing basalt fiber has a better effect on improving the compressive strength of concrete than splitting tensile strength. Through the analysis of the corrosion resistance coefficient of compressive strength, the corrosion resistance coefficient of splitting tensile strength, and the relative dynamic elastic modulus of BFRC, it was found that basalt fiber has good compatibility with the concrete matrix and the deterioration degree of BFRC is lower than that of ordinary concrete.
- (5) Based on the SEM micro-analysis, the sulfate corrosion products are mainly gypsum and ettringite. These products jointly fill the internal pores of the BFRC at the initial stage. With dry–wet cycles, there are not enough pores inside the BFRC to accommodate these products. The increased stress leads to the decrease of mechanical properties; the deterioration degree is serious.

Funding Statement: Financial supports for the study were provided by the Natural Sciences Foundation Committee of China (Grant No. 41472254, Jinming Xu, <http://www.nsf.gov.cn>).

Conflicts of Interest: The authors declare that they have no conflicts of interest to report regarding the present study.

References

1. Fazilati, M., Golafshani, E. M. (2020). Durability properties of concrete containing amorphous silicate tuff as a type of natural cementitious material. *Construction and Building Materials*, 230, 117087. DOI 10.1016/j.conbuildmat.2019.117087.
2. Gangnant, A., Saliba, J., La Borderie, C., Morel, S. (2016). Modeling of the quasibrittle fracture of concrete at meso-scale: Effect of classes of aggregates on global and local behavior. *Cement and Concrete Research*, 89, 35–44. DOI 10.1016/j.cemconres.2016.07.010.
3. Gao, R. D., Li, Q. B., Zhao, S. B., Yang, X. M. (2010). Deterioration mechanisms of sulfate attack on concrete under alternate action. *Journal of Wuhan University of Technology (Materials Science)*, 25(2), 355–359. DOI 10.1007/s11595-010-2355-2.
4. Gao, J. M., Yu, Z. X., Song, L. G., Wang, T. X., Wei, S. (2013). Durability of concrete exposed to sulfate attack under flexural loading and drying–wetting cycles. *Construction and Building Materials*, 39, 33–38. DOI 10.1016/j.conbuildmat.2012.05.033.
5. Bassuoni, M. T., Nehdi, M. L. (2008). Durability of self-consolidating concrete to sulfate attack under combined cyclic environments and flexural loading. *Cement and Concrete Research*, 39(3), 206–226. DOI 10.1016/j.cemconres.2008.12.003.
6. Zhang, Z. Y., Zhou, J. T., Zou, Y., Yang, J., Jin, X. G. (2020). Effect of sulfate attack on the shear performance of concrete. *China Civil Engineering Journal*, 53(7), 64–72. DOI 10.15951/j.tmgcxb.2020.07.005.

7. Jiang, L., Niu, D. T. (2015). Damage layer and microscopic analysis of concrete under sulfate attack. *Bulletin of the Chinese Ceramic Society*, 34(12), 3462–3467. DOI 10.16552/j.cnki.issn1001-1625.2015.12.012.
8. Zheng, Y. X., Zhuo, J. B., Zhang, P. (2021). A review on durability of nano-SiO₂ and basalt fiber modified recycled aggregate concrete. *Construction and Building Materials*, 304, 124659. DOI 10.1016/j.conbuildmat.2021.124659.
9. Huang, M., Zhao, Y. R., Wang, H. N., Lin, S. H. (2021). Mechanical properties test and strength prediction on basalt fiber reinforced recycled concrete. *Advances in Civil Engineering*, 2021, 6673416. DOI 10.1155/2021/6673416.
10. Wang, X. Z., He, J., Mosallam, A. S., Li, C. X., Xin, H. H. et al. (2019). The effects of fiber length and volume on material properties and crack resistance of basalt fiber reinforced concrete (BFRC). *Advances in Materials Science and Engineering*, 2019, 7520549. DOI 10.1155/2019/7520549.
11. Li, W. M., Xu, J. Y. (2008). Strengthening and toughening in basalt fiber-reinforced concrete. *Journal of the Chinese Ceramic Society*, (4), 476–481+486. DOI 10.3321/j.issn:0454-5648.2008.04.009.
12. Yang, L. Y., Xie, H. Z., Fang, S. Z., Huang, C., Yang, A. et al. (2021). Experimental study on mechanical properties and damage mechanism of basalt fiber reinforced concrete under uniaxial compression. *Structures*, 31, 330–340. DOI 10.1016/j.istruc.2021.01.071.
13. Chen, F., Chen, X. (2014). Orthogonal experimental of strength of concrete reinforced by basalt fibre. *Journal of Fuzhou University (Natural Science Edition)*, 42(1), 133–137. DOI 10.7631/issn.1000-2243.2014.01.0.
14. Branston, J., Das, S., Kenno, S. Y., Taylor, C. (2016). Influence of basalt fibres on free and restrained plastic shrinkage. *Cement and Concrete Composites*, 74, 182–190. DOI 10.1016/j.cemconcomp.2016.10.004.
15. Lee, J. J., Song, J. Y., Kim, H. D. (2014). Chemical stability of basalt fiber in alkaline solution. *Fibers and Polymers*, 15(11), 2329–2334. DOI 10.1007/s12221-014-2329-7.
16. Jalasutram, S., Sahoo, D. R., Matsagar, V. (2017). Experimental investigation of the mechanical properties of basalt fiber-reinforced concrete. *Structural Concrete*, 18(2), 292–302. DOI 10.1002/suco.201500216.
17. Wang, Z. S., Xing, L. X., Zhao, K., Lu, J. L., Tian, J. B. (2020). Research on corrosion resistance and mechanical properties deterioration of basalt fiber reinforced concrete under magnesium sulfate erosion environment. *Chinese Journal of Applied Mechanics*, 37(1), 134–141+477. DOI 10.11776/cjam.37.01.D101.
18. Han, X., Zhan, S., Xu, Q., Tang, X., Wang, L. et al. (2020). Effect of dry-wet cycling on resistance of concrete to chloride ion permeation erosion. *Acta Materiae Compositae Sinica*, 37, 198–204. DOI 10.13801/j.cnki.fhclxb.20190402.005.
19. Ma, Y. P., Yu, S. T., You, L., Meng, R., Yang, X. J. (2018). Effect of fiber parameters on crack reduction of cement based materials. *Journal of Building Materials*, 21(5), 797–802. DOI 10.3969/j.issn.1007-9629.2018.05.016.
20. Wang, Z. S., Li, Y. K., Lu, J. L., Tian, J. B., Zhao, K. (2020). Research on corrosion characteristics and performance degradation of basalt fiber concrete under sodium magnesium sulfate corrosion environment. *Journal of Coastal Research*, 111(sp1), 56–62. DOI 10.2112/JCR-SI111-010.1.
21. Luo, Y., Niu, D., Su, L. (2021). Chloride diffusion property of hybrid basalt-polypropylene fibre-reinforced concrete in a chloride-sulphate composite environment under drying-wetting cycles. *Materials*, 14(5), 1138. DOI 10.3390/ma14051138.
22. He, S. Q., Wang, H. C. (2003). Orthogonal experimental studies on mix design of high performance concrete. *Industrial Construction*, 8, 8–10+41. DOI 10.3321/j.issn:1000-8993.2003.08.003.
23. Chen, X., Xu, B., Xu, B. (2012). Predicting the deformation of roller compacted concrete dam using least squares support vector machine. *Journal of Food, Agriculture & Environment*, 10(3&4), 1376–1378.